Scientia Iranica B (2015) 22(5), 1918–1930

SCIENTIA IRANICA

Sharif University of Technology
Scientia Iranica
Transactions B: Mechanical Engineering
www.scientiairanica.com

Research Note

Analysis of hydrodynamics and noise prediction of the marine propellers under cavitating and non-cavitating conditions

M.R. Bagheri[a], M.S. Seif[a,*], H. Mehdigholi[a] and O. Yaakob[b]

a. *The Centre of Excellence in Hydrodynamics and Dynamic of Marine Vehicles, Sharif University of Technology, Tehran, Iran.*
b. *Marine Technology Centre, Universiti Teknologi Malaysia, 81310 UTM Skudai, Malaysia.*

Received 28 June 2014; received in revised form 14 December 2014; accepted 26 January 2015

KEYWORDS
FVM;
FW-H;
Cavitation;
Propeller hydrodynamics;
Propeller noise.

Abstract. Marine propeller hydrodynamics and noise study is an important issue in considering the suitable performance of the ships and submarines. At the first step of this study, the hydrodynamics of two propellers was studied under different operating conditions. Then the sheet cavitation inception and development conditions were obtained in order to determine the impact of varying rotational speeds of the propeller and pressure drop on the propeller noise. At the second step, the overall Sound Pressure Levels (SPLs) for each one of these models were extracted under non-cavitating and sheet cavitating conditions. The overall SPLs were calculated through the Ffowcs Williams-Hawkings (FW-H) equation and its integral solutions. In this work, the flow field was analysed through the FVM, and then the flow data, including pressure fluctuations, sheet cavitation volume, and velocity magnitude results of the flow solution were used as the inputs for the FW-H formulation to predict the overall SPLs. The results of the flow analysis are significant since they are used as the noise sources in the FW-H equations to obtain the overall SPLs. Therefore, these results must be thoroughly analysed. The numerical hydrodynamic results were compared with the experimental results from the two propellers and a good coordination was found.

1. Introduction

The three major sources of underwater noise, produced by the underwater and surface vehicles, are the machinery, propeller, and flow noise. There are four mechanisms which produce the propeller pressure waves [1,2]. Cavitation noise is the major source of noise from the propeller and should be thoroughly investigated. Since cavitation noise is the major source of propeller noise, it should be analysed accurately. There are various ways to evaluate sound equation and the three types of noise source terms (monopole, dipole and quadruple).

Seol et al., in 2002, presented a study on the non-cavitating underwater propeller noise [3] while in [4], in 2005, they described the use of a hybrid method to predict the underwater propeller noise in non-cavitating and cavitating conditions [4]. They examined a DTMB4119 model, and the results were presented in only one operating condition and for a low frequency range. The noise of a DTMB4118 propeller was investigated by Jin-Ming et al. in 2012 [5]. They concluded that the overall spectrum amplitude of the sound in front of the propeller hub is more than in the propeller rotational plane. In 2013, PAN et al. [6] also evaluated the marine propeller noise in non-uniform

*. *Corresponding author. Tel.: +98 21 66165549; Fax: +98 21 66000021*
E-mail address: seif@sharif.edu (M.S. Seif)

flow through FW-H equation. There are various ways to evaluate the FW-H equation. In certain studies [3-6], the FW-H equation has been solved using the panel method.

Other research has been performed using commercial codes like CFD and FLUENT. They used the Reynolds-Averaged Navier-Stokes (RANS) equation solver for flow field analysis in order to extract the SPLs. In 2007, Caro et al. presented a CAA formulation based on Lighthill's analogy for fan noise using the CFD method [7], and in 2008, CHEN et al. investigated a numerical analysis for the aerodynamic noise radiated from the cross flow fan [8]. Li et al., in 2010, presented experimental and numerical studies on the discrete noise of the cross-flow fan with block-shifted impellers [9]. In 2011, Lai et al. studied the attenuation of the cross-flow fan noise using porous stabilisers [10], and Rama et al. considered the motor fan noise reduction using CFD and CAA simulations [11]. Gue et al., in 2011, presented the development of low-noise axial cooling fans in a household refrigerator [12]. The flow field results include pressure fluctuations, sheet cavitation fluctuations, and velocity magnitude. These are used as the inputs for predicting the noise analysis under non-cavitating and cavitating conditions. Therefore, flow results should be correctly obtained and then be compared in experiment.

Li and Yang, in 2009, investigated the numerical simulation of the flow around a propeller. Their studies were performed using the commercial CFD software FLUENT; they also used a standard $k-\varepsilon$ model with wall functions [13]. Subhas et al., in 2012, presented the analysis of a propeller's flow and cavitation [14]. In their research, the CFD code Fluent 6.3 software was used to solve advanced phenomena like cavitation of the propeller. Their investigations were based on a standard $k-\varepsilon$ turbulence model in combination with a volume of fluid implementation to capture the interface between liquid and vapour. Sanchez, in 1998, calculated the open water flow patterns and performance coefficients for a DTRC 4119 propeller using FINFLO code [15]. The flow patterns were generally predicted using the $k-\varepsilon$ turbulent model. Bagheri et al., in 2012 and 2013, studied the non-cavitating and cavitating noise and hydrodynamics of the marine propellers using FVM by the RNG $k-\varepsilon$ turbulent model [16,17].

The FW-H formulation adopts the most general form of Lighthill's acoustic analogy and is capable of predicting the generated sound by equivalent acoustic sources such as monopoles, dipoles, and quadruples. The FW-H acoustics model in ANSYS/FLUENT14.5 code allows one to select multiple source surfaces and receivers. As mentioned earlier, when cavitation happens, sheet cavitation is the main sound source in low frequency ranges. Therefore, it should be modelled accurately in numerical simulations. Senocak and Shyy, in 2001, presented a numerical simulation of turbulent flows by sheet cavitation [18]. Pereira et al., in 2004, presented an experimental and theoretical study on a cavitating propeller in uniform inflow [19]. Bernad, in 2006, presented a numerical investigation of the cavitating flows using the mixture model implemented in the Fluent 6.2 commercial code [20]. Sridhar et al., in 2010, predicted the frictional resistance offered to a ship in motion using Fluent 6.0 and the results are validated by the experimental results [21]. Salvatore et al., in 2011, presented a computational analysis of the marine propeller performance and cavitation by using an inviscid-flow BEM model [22]. Zhu et al., in 2012, investigated the cavitation performance of propellers using the viscous multiphase flow theories and with a hybrid grid based on Navier-Stokes equations [23]. In certain studies [18-23], the most advanced computational tools for sheet cavitation analysis on marine propellers are based on the RANS equations. RANS codes can predict velocity distribution in the propeller accurately while the accuracy of the velocity predictions by the panel method is not adequate because of lack of the viscous effect in the theory [24]. Therefore, in this work, the flow field was analysed by solving the RANS equation.

As mentioned, much experimental research has been conducted to measure the propeller noise and hydrodynamics in the cavitation tunnel. Sharma et al., in 1990, investigated some marine propellers in the cavitation tunnel [25]. In their study [25], the differences between the noise levels under non-cavitating and cavitating conditions were reported within the range of 10 to 30 dB. Atlar et al., in 2001, investigated cavitation tunnel tests for the propeller noise of a FRV [26]. Park et al., in 2009, studied noise source localization in a cavitation tunnel [27]. They concluded that vortex cavitation detaching from sheet cavitation causes increases in the noise levels within high frequency ranges, and that large noises in low frequencies are due to the increases in the volumes of sheet cavitation on the propeller blade surfaces which act like large vibrating bubbles [27]. Bagheri et al., in 2014, studied hydrodynamics and noise prediction of a marine propeller by numerical and experimental methods [28]. In the present study, we investigated the sheet cavitation effects on the overall increase in SPLs as the most important sound sources under cavitation in low frequencies. In this paper, the acoustic field and hydrodynamic analysis of two marine propellers is presented in a uniform flow by FVM in ANSYS/FLUENT14.5 commercial code. Moreover, various parameters such as inlet velocity, propeller rotational speed, and pressure drop are investigated

to elicit the conditions of sheet cavitation inception and development and the sheet cavitation effects on the overall SPLs. Also, sudden pressure changes are considered in sheet cavitation development and their effects on the overall noise of the propeller are studied. The results from the flow analysis are significant since they are used as the noise sources in the FW-H equations for obtaining the overall SPLs, and therefore, these results must be thoroughly analysed. The flow field is investigated by solving the RANS equation and using the Zwart cavitation model. The hydrodynamics and sheet cavitation results are compared and verified against the experimental findings for two propellers. Then the overall noise results of the propeller are extracted using the FW-H equation by FVM. Acoustic results for a three-blade propeller are extracted in various operating conditions, and then the overall SPL is verified using methods from previous studies done in similar conditions. In the present work, the results are presented for different operating conditions.

2. Methodology

The basic equation for sound propagation is the Lighthill equation obtained from the continuity and momentum equations [29]. The FW-H is a solution developed from the Lighthill equation. In the FVM, the FW-H formulation is used to extract the overall SPLs in the far field. ANSYS/FLUENT14.5 offers a method based on the FW-H equation and its integral solutions. The FW-H formulation is represented by Eq. (1) [30]:

$$\frac{1}{c_0^2}\frac{\partial^2 p'}{\partial t^2} - \nabla^2 p' = \frac{\partial^2}{\partial x_i x_j}\left[T_{ij}H(f)\right] - \frac{\partial}{\partial x_i}\left([P_{ij}n_j + \rho u_i(u_n - v_n)]\delta(f)\right) + \frac{\partial}{\partial t}\left(\rho_0 v_n + \rho(u_n - v_n)\right)\delta(f). \quad (1)$$

The terms in the right side of Eq. (1) are called quadruple, dipole, and monopole sources, respectively. p' is the sound pressure at the far-field ($p' = p - p_0$). Setting $f = 0$ introduces a surface that embeds the external flow ($f > 0$) effect, while c_0 is the far-field sound speed and T_{ij} is the Lighthill stress tensor [29]. $H(f)$ and $\delta(f)$ are Heaviside and Dirac delta functions, respectively [30]. Farassat proposed the Formulation 1A in [31] for solving the FW-H equation within the time domain. In the Farassat's formulation, the pressure field is defined by Eqs. (2) to (4):

$$P'(\vec{x},t) = P'_T(\vec{x},t) + P'_L(\vec{x},t), \quad (2)$$

$$4\pi P'_L(\vec{x},t) = \int_{f=0}\left[\frac{\rho_0 \frac{\partial v_n}{\partial t}}{r(1-M_r)^2}\right]_{ret} dS + \int_{f=0}\left[\frac{\rho_0 \frac{v_n}{\partial t}(r\frac{\partial M_1}{\partial t}\hat{r}_i + c_0 M_r - c_0 M^2)}{r^2(1-M_r)^3}\right]_{ret} dS, \quad (3)$$

$$4\pi P'_L(\vec{x},t) = \frac{1}{c_0}\int_{f=0}\left[\frac{l_1\hat{r}_i}{r(1-M_r)^2}\right]_{ret} dS + \int_{f=0}\left[\frac{l_r - l_i M_i}{r^2(1-M_r)^2}\right]_{ret} dS + \frac{1}{c_0}\int_{f=0}\left[\frac{\rho_0 v_n(r\frac{\partial M_1}{\partial t}\hat{r}_i + c_0 M_r - c_0 M^2)}{r^2(1-M_r)^3}\right]_{ret} dS, \quad (4)$$

where P' is the acoustic pressure; P'_T and P'_L describe the acoustic pressure field resulting from thickness and loading, corresponding to the monopole and the dipole sources; e.g. blade rotation and unsteady sheet cavitation on the blades are defined as monopole sources and fluctuation pressure on the blade surface is defined as a dipole source; $r(= |x(t) - y(\tau)|)$ is the distance between the receiver and the source; x and t are the sound receiver's position and time, respectively; also y and τ are the source's position and time, respectively; M is the Mach number; $M_r = M_i\hat{r}_i$ is the component of the Mach number vector in the direction of the receiver; and $r'_i = r_i/r$ defines the unit vector in the radiation direction; l_i is the local force per unit area in direction i; v is the local normal velocity of the blade surface; and $c_0 = 1500$ m/s and $\rho_0 = 1025$ kg/m^3 are the sound speed and density in water.

In the present study, the first flow around the object is obtained to determine the sources of noise. Flow results as the blade rotation effect in water, unsteady sheet cavitation, and fluctuation pressure on the blade surface are used as the inputs for noise analysis. The flow field of the propeller is obtained using FVM through the solution of the RANS equations. The FW-H acoustics model in ANSYS/FLUENT14.5 code allows you to select multiple source surfaces and receivers. In this work, the surfaces of the propeller blades are selected by integral surfaces, $f = 0$, in Eqs. (3) and (4). The main objective of the cavitation physical model is to extract mass fraction of the vapour and liquid phases. In this study, a multi-phase method is used in order to extract the vapour volume fraction [32].

3. Numerical analysis, model geometry, and grid generation

In this study, four- and three-blade propellers are used which will be called A and B models, respectively,

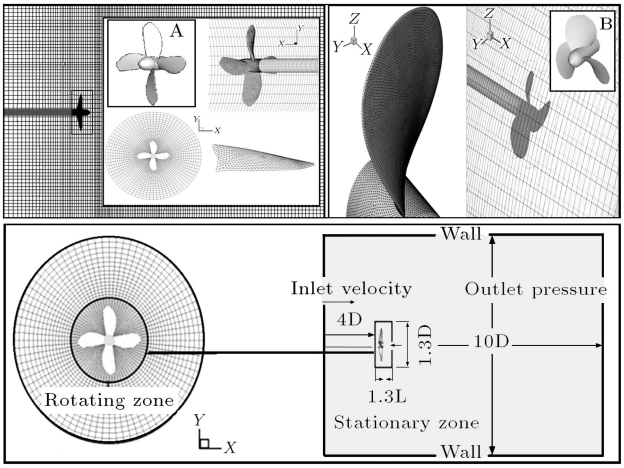

Figure 1. Geometry of the model, grids of Models A and B, computational domain, and boundary conditions.

hereafter. Model A was designed at the Centre of Excellence in Hydrodynamics and Dynamic of Marine Vehicles (CEHDMV) and this model is similar to the B-series. This model is a research model with high application at CEHDMV. It provided the necessary noise measurements for us. Model B is a DTMB4119 that has been analysed in numerous studies. Figure 1 presents the information and several quantities, such as the geometries of the models, surface grids on the hub and blade surfaces, the computational domains of the solution field, and the boundary conditions. In this study, we use the same modelling approach, turbulence model and numerical solution method as in the studies [7-23], but with the intention of reaching higher goals.

The boundary conditions and the solution domain size are the same for both the models. The main contributing parameters in the accuracy of a numerical simulation of any geometry are the type of cells, size of meshes, and quality, since their compositions affect the convergence/divergence of the solution to a great extent. The blade surface is meshed with triangle grids. The zone around the root, tip, and blade edges is meshed with smaller triangles, i.e. with sides of approximately $0.001D$. The $y+$ value gives important information about the resolution of the boundary layer. Value of the coefficient $y+$ was the main criterion for setting the mesh resolution. The coefficient should be in a range of $30 < y+ < 500$ [33,34] in order to properly model the turbulent boundary layer and obtain correct pressure distributions on the propeller blade surfaces for the $k-\varepsilon$ model. The $y+$ value along the propeller surface was around +30 to 295 for Model A. But for Model B, the $y+$ value was obtained in a range of $36 < y+ < 306$ which is in the range of reference [34]. Therefore, the appropriate $y+$ value is in a range of $30 < y+ < 300$ for both models.

Each propeller has been simulated with various grids. First, number of the meshes was considered 543,406 for Model A. With this number of meshes, vapour volume fraction on the blade surface did not occur despite the experimental results in the reference [35]. Therefore, in order to observe the vapour volume fraction on the blade surface, the number of cells was increased from 543,406 to 1,176,450 on the propeller surface. In this condition, cavitation or vapour volume fraction occurred on the blade surface in $j = 0.22$ for Model A. Then, in order to consider the grid independence, we considered the pressure coefficient (Cp) for an additional three sets of grids, grids 1, 2, and 3, containing 1,176,450, 2,000,000, and 2,332,800 meshes, respectively. In these sets of grids, we mostly refined the edge and tip of the blades which is important in simulation of the propeller cavitation. Figure 2 shows the Pressure distribution for $r/R = 0.7$ in different grids of Model A. As shown in this figure, the pressure coefficient did not change for this model when the number of grids increased from 2,000,000 to 2,332,800 meshes. Therefore, the number of 2,000,000 cells was selected for Model A and the results are presented for this number of meshes. The grid independency for Model B is considered similar to Model A. Grids 1, 2 and 3 contained 3,870,000,000, 5,000,00,0 and 5,453,000 meshes in Model B, respectively. Figure 3 shows the Pressure distribution for $r/R = 0.7$ in

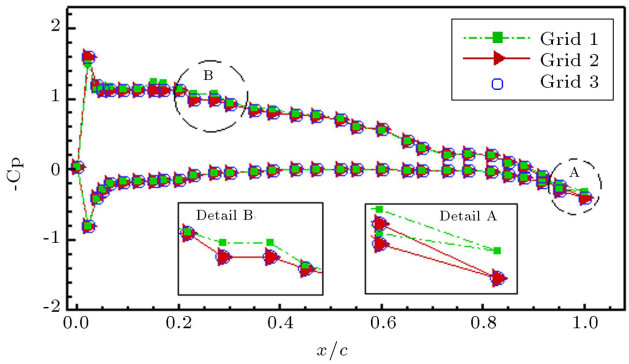

Figure 2. Pressure distribution for $r/R = 0.7$ in different grids of Model A.

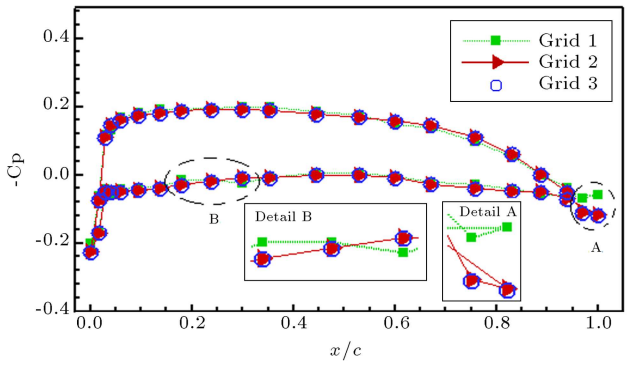

Figure 3. Pressure distribution for $r/R = 0.7$ in different grids of Model B.

different grids of Model B. As shown in this figure, the pressure coefficient was constant for this model when the number of grids increased from 5,000,000 to 5,453,000 meshes. Finally, the appropriate numbers for grids were selected at 2,000,000 and 5,000,000 cells for Models A and B, respectively.

The solution field of flow around the propeller was divided into two zones. The rotating zone contains the flow around the propeller and the stationary zone contains the flow around the moving zone. A cylindrical shape was assumed for the rotating zone with a length $1.06D$ times the propeller diameter, and a width of $1.06L$ in which L is the hub length. This zone should be considered small, limited to rotational zone dimensions. The rotating zone was solved via the Moving Reference Frame, MRF. The inlet was situated in $4D$ distance in the upstream, while the outlet was located at $10D$ downstream and the outer boundary was at $5D$ from the shaft axis, as can be seen in Figure 1. In order to simulate the flow around the rotating propeller where the inlet boundary was located, we have imposed the velocity components for a uniform stream with a given inflow speed. At the blade and hub surface, a wall condition has been considered, while a wall boundary condition and constant pressure conditions were imposed on the lateral and outlet boundaries, respectively.

In order to discrete the convective terms, the second order is used with an accurate upwind scheme while the velocity-pressure coupling and the overall solution procedure were based on the SIMPLEC type. The cavitation is an unsteady phenomenon and so this problem is solved in the unsteady state. The solution for the Unsteady Reynolds-Averaged Navier-Stokes (URANS) equations was to utilise the RNG $k-\varepsilon$ turbulence model and the FW-H sound equation was performed by the ANSYS/Fluent14.5. In this paper, the RNG $k-\varepsilon$ turbulence model is used for the URANS equations. Although the RNG $k-\varepsilon$ model is based on the standard $k-\varepsilon$ model, it has many advantages [33].

4. Hydrodynamic results and discussion

Model A. Model A is a research propeller used in the CEHDMV in Sharif University of Technology. Hydrodynamic tests on this propeller have been performed in the k23 cavitation tunnel at CEHDMV [35]. Model A has $D = 0.29$ m, EAR=0.43, and $r_h/R = 0.17$; these characteristics are, geometrically, similar to the B-series [2]. Numerical results of this paper were compared with experimental results in [35] for this model. The effect of changing rotational speed and pressure drop for sheet cavitation development was analysed for this model.

K_T, K_Q, and η_0 have been calculated, using a numerical method, and compared with experimental tests for all the cases [35]. The curve in Figure 4 shows the hydrodynamic characteristics of Model A for the numerical and experimental results. Figure 4 suggests that a good coordination is found between the numerical and experimental results in a variety of operating conditions.

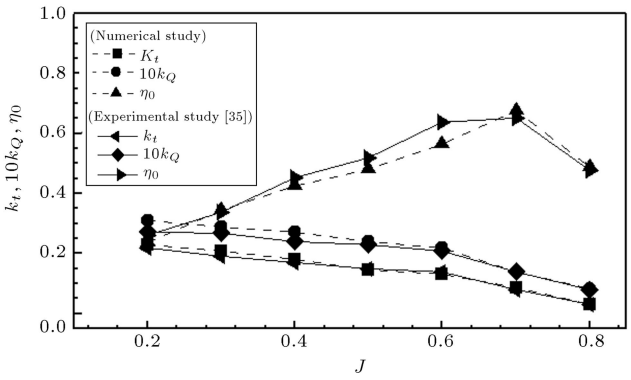

Figure 4. Comparison of the hydrodynamic characteristic curves between the numerical and experimental analyses of Model A.

Sheet cavitation is one of the most important propeller noise sources in low frequency ranges, and therefore, its inception and development conditions should be obtained. In the present study, a computational method for analysis of the propeller noise was used. Flow results, cavity volume fluctuations, and blade surface pressure data are used as the inputs for noise analysis under cavitation conditions. Among the various types of cavitation noise, unsteady sheet cavitation on the blade surface is known to produce the highest noise level in low frequencies [4,27]. In these simulations, sheet cavitation is presented as the most important source of propeller noise in cavitation conditions. Figure 5 shows the qualitative comparison between the experimental and numerical results of the sheet cavitation. The cavity pattern generally agrees well with the experiments, and also the sheet cavity shape on the blade surface is well-reproduced. Under

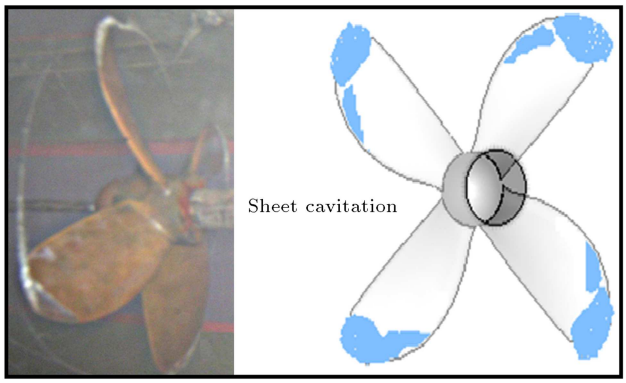

Figure 5. Comparison between the simulated and experimental [35] results of sheet cavitation on the blades of Model A in $N = 900$ rpm and $P_{op} = 60$ kPa.

Table 1. The cavitation numbers in different points of Model A

J	S	σ	J	S	σ	J	S	σ
	R	0.85		R	0.004		R	0.002
$J = 0.22$	$0.7R$	0.98	$J = 0.166$	$0.7R$	0.380	$J = 0.125$	$0.7R$	0.180
	0	7.870		0	7.600		0	2.040

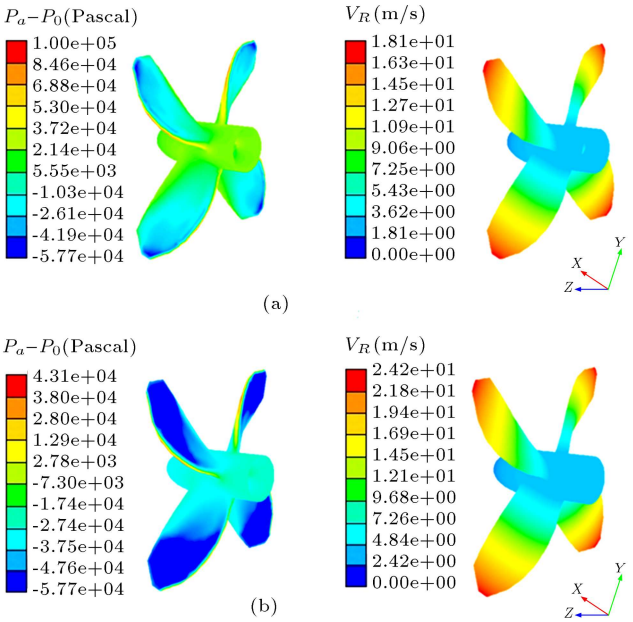

Figure 6. The contours of relative pressure (pa) and flow velocity (m/s) for Model A at (a) $J = 0.166$, and (b) $J = 0.125$ in $P_{op} = 101$ kPa.

these conditions, cavitation was started and expanded as the propeller rotational speed increased.

For the sake of comparison, cavitation development is considered under different conditions; $N = 900$ rpm, $N = 1200$ rpm, and $N = 1600$ rpm with a constant water speed of $V = 1$ m/s. Figure 6 presents the velocity magnitude and relative pressure contours for each of these three cases. Obtaining values from these contours, cavitation number can then be calculated from Eq. (5). The acquired data implies that a vapour phase should exist at the tip and at all the located points at 0.7R on the hub axis [2].

$$\sigma_{0.7R} = \frac{P_{\text{static}} - P_v}{0.5\rho V_R^2},$$

$$V_R = \sqrt{V_a^2 + (0.7Rw)^2},$$

$$P_{\text{static}} = (P_0 - P_a)_{\text{numerical}} + P_{op}, \tag{5}$$

where V_a and w are water speed (m/s) and the propeller rotational speed (rad/s), respectively; ρ is the water density (kg/m^3); P_{static}, P_v, P_{op} and $P_0 - P_a$ are the static pressure (P_a), water vapour pressure (P_a), operational pressure (P_a), and the obtained relative pressure in numerical results from Figure 6, respectively. The

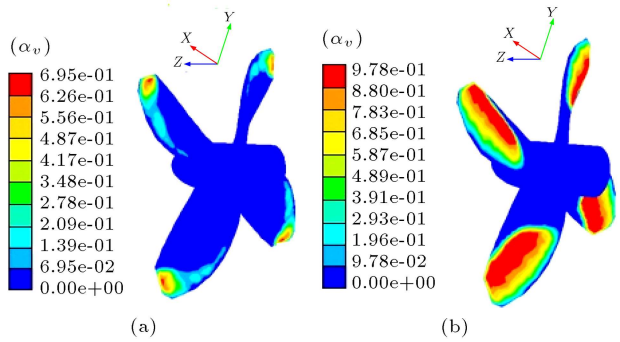

Figure 7. Vapour volume fraction of Model A at (a) $J = 0.166$, and (b) $J = 0.125$ in $P_{op} = 101$ kPa.

results of cavitation numbers, σ, at different points of the blade are presented in Table 1. Injecting and expanding the vapour volume fraction in the fluid increases the overall noise, because cavitation is one of the most important noise sources of the propeller.

Figure 7 shows the sheet cavitation development and the vapour volume fraction resulting from the increase in the rotational speed of the propeller when $N = 1200$ rpm and $N = 1600$ rpm. In this figure, the vapour volume fraction on the surface of the blades dramatically increases, especially when the rotational speed increases from 1200 rpm to 1600 rpm. Increase in the vapour volume fraction plays an important role in producing noise in the fluid which will be discussed in Section 5.

Model B. Model B has been numerously analysed in the ITTC committee. The main objective for the analysis of Model B in this paper is to study the sheet cavitation inception and its effects on the overall SPLs of the propeller. Initially the propeller rotational speed was set at 120 rpm under an inlet velocity of 1.6 m/s and an operating pressure of $P_{op} = 101$ kPa. Subsequently, the pressure was reduced to 60 kPa in order to observe the impacts on the overall SPLs, while rotational and flow speed were kept at 120 rpm and 1.6 m/s, respectively. This model is considered particularly for sheet cavitation inception at super high rotational speeds. In the first case, the operational pressure was kept at $P_{op} = 60$ kPa, and the impact of changing the rotational speed and increasing the vapour volume fraction on cavitation development was studied. Figure 8 presents the curve associated with the hydrodynamic characteristics of Model B in the numerical analysis; these

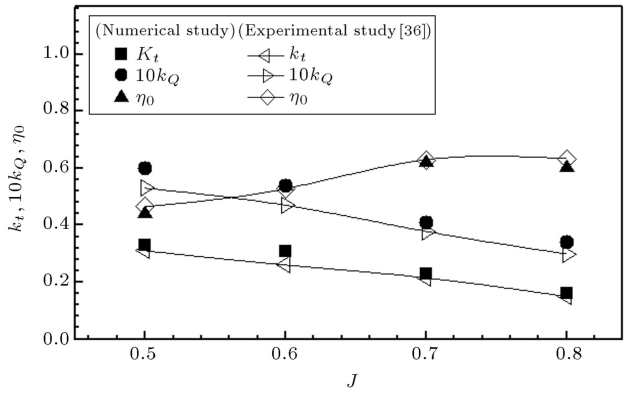

Figure 8. Comparison of the hydrodynamic characteristic curves between the numerical and experimental analyses of Model B in numerical and experimental analysis.

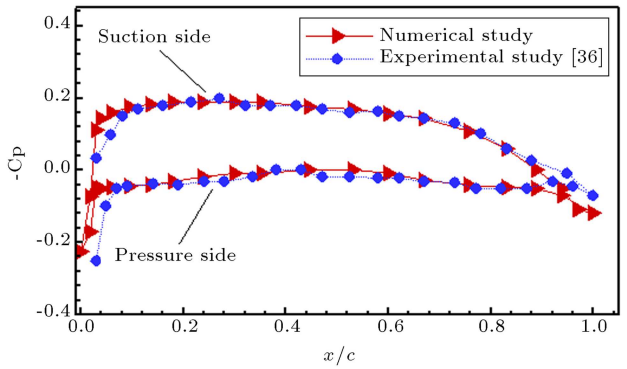

Figure 9. Comparison of pressure distribution in numerical and experimental analyses for $r/R = 0.7$ in $j = 0.8$.

characteristics are compared with experimental results in [36]. Figure 9 presents a comparison between the Pressure distributions in the numerical and experimental analyses for $r/R = 0.7$. In this figures, there is good agreement between hydrodynamic numerical and experimental results. In the present work, two parameters are considered in order to obtain sheet cavitation inception conditions, including the increase of propeller rotational speed in constant operating pressure and the drop pressure in constant rotational speed. The first rotational speed was considered at 120 rpm, and then it was increased in the range of 120 rpm to 1850 rpm at constant operating pressure, $P_{op} = 101$ kPa. Cavitation finally started in 1850 rpm for $P_{op} = 101$ kPa.

On the other hand, when the operating pressure decreased, cavitation happened in lower rotational speeds. This illustrates that cavitation can be formed in lower rotational speeds if operating pressure is dropped. Figure 10 shows the velocity magnitude and relative pressure contours for Model B in $N = 1850$ rpm and $V = 2.96$ m/s which are used to calculate the cavitation number. Figure 11 depicts the vapour volume fraction contour for $N = 1850$ rpm and $V = 2.96$ m/s. As this figure shows, the sheet cavitation is low on the tip of the blades.

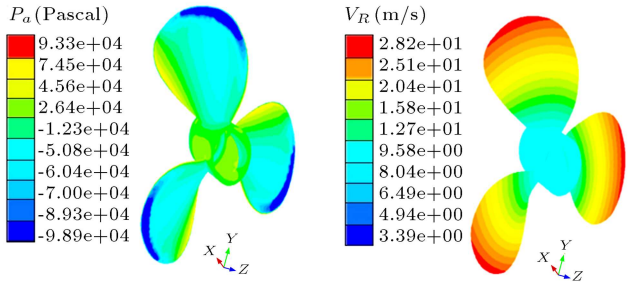

Figure 10. The contours of relative pressure (Pa) and flow velocity (m/s) for Model B ($N = 1850$ rpm, $V = 2.96$ m/s and $J = 0.32$).

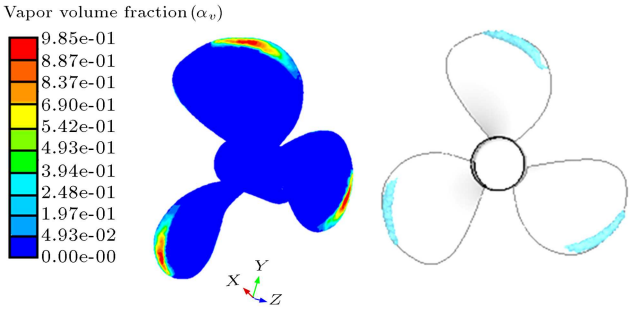

Figure 11. Vapour volume fraction of Model B at $N = 1850$ rpm and $V = 2.96$ m/s.

In this section, the flow around the propeller was solved using RANS equations, and then the flow data were used as the inputs for FW-H equation to predict the far-field acoustics. In the next sections, the overall SPLs results will be presented under non-cavitating and sheet cavitating conditions for the two models using solution of FW-H equations in FVM.

5. Acoustic results

5.1. The overall SPLs results under non-cavitating conditions

As mentioned earlier, the flow field results are used as the inputs for the FW-H solution in the ANSYS/FLUENT14.5 code. In other words, the presented overall SPLs in this paper include not only the cavitation effects, but also all other sound sources. In this paper, the goal is to elicit the overall SPLs under non-cavitating and cavitating conditions. Four hydrophones were used to extract the overall SPLs for the acoustic simulations of Models A and B. The hydrophones position is shown in Figure 12.

Figure 13 shows the overall SPLs for Model A under a non-cavitating condition at $j = 0.66$, $N = 900$ rpm, $V = 3$ m/s, and $P_{op} = 101$ kPa. This figure shows the overall SPLs at two different distances of $5R$ and $10R$ for hydrophones 3 and 4. The results from these hydrophones show a peak at 60 Hz frequency for

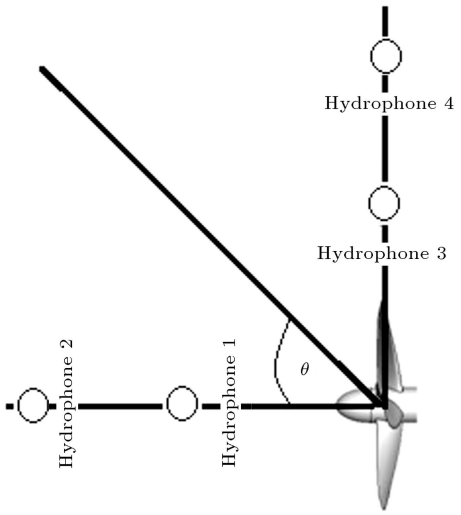

Figure 12. Position of hydrophones in Models A and B.

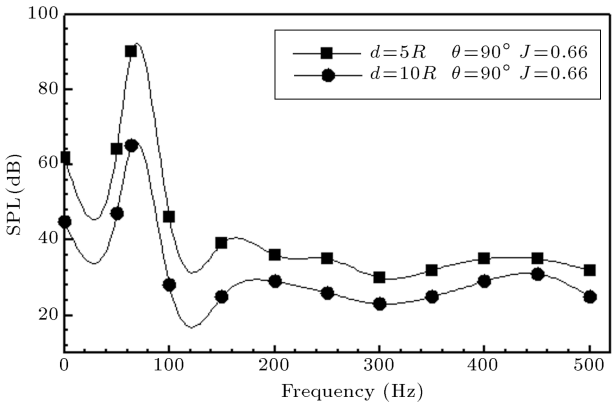

Figure 13. Overall SPLs under non-cavitating conditions for hydrophones 3 and 4 of Model A; $N = 900$ rpm and $V = 3$ m/s.

Model A which is in accordance with Eq. (6) related to the first Blade Passing Frequency (BPF) of the propeller; see Figure 13 for the overall SPL [37].

$$f_m = mzf_r, \tag{6}$$

where m is the harmonic number, z is the number of blades, and f_r is the rotational frequency of the shaft [2].

Figure 14 shows the overall SPLs at distances of $5R$ and $10R$ for hydrophones 1 and 2 in front of the hub on the z-axis at $j = 0.66$. Comparing Figures 13 and 14, it can be deduced that the overall SPL is higher in front of the hub compared to the amount in the propeller rotational plane.

As illustrated by Figures 13 and 14, the overall SPL reduces as the distance from the sound source increases. In the far field where sound propagates as spherical waves and $kr >> 1$, k is the wave number and r is the distance to sound source; sound pressure follows the inverse square law with respect to the

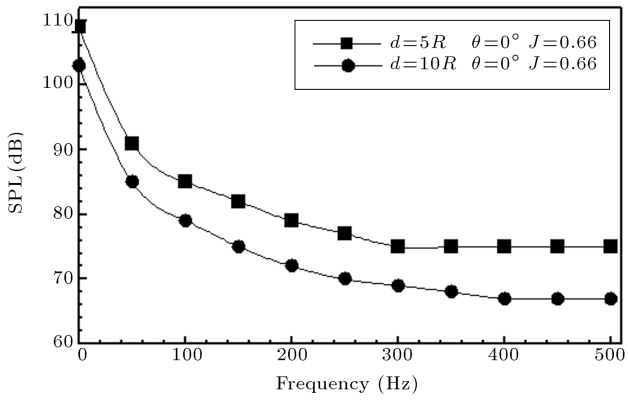

Figure 14. Overall SPLs under non-cavitating conditions for hydrophones 1 and 2 of Model A; $N = 900$ rpm and $V = 3$ m/s.

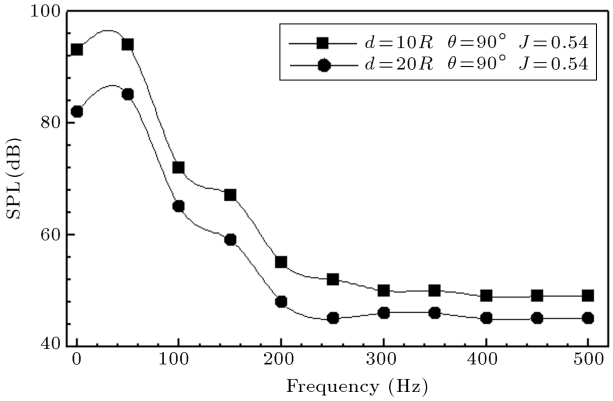

Figure 15. Overall SPLs under non-cavitating conditions for hydrophones 3 and 4 of Model B; $N = 960$ rpm and $V = 2.6$ m/s.

distance [37]. In other words, in the far-field, the overall SPL is related to the inverse square of the distance. For example, if the distance doubles, the overall SPL decreases around 6 to 7 dB. Therefore, one can use this relationship in order to find the suitable amplitude for the far-field. Figure 14 shows that for each frequency, the difference between the overall SPLs of hydrophones 1 and 2 is from 6 to 8 dB. Therefore, distances greater than 10R could be considered as far field. This phenomenon has been previously verified by [5]. Figures 15 and 16 show the overall SPL results for Model **B** at $N = 960$ rpm. For this model, the inverse square law and overall SPL spectrum results are similar to the results of Model A.

5.2. Overall SPL results under cavitating conditions

5.2.1. Model A

As mentioned in Section 4, sheet cavitation happens at $N = 900$ rpm when $P_{op} = 60$ kPa; see Figure 5. By increase in rotational speed in constant operating pressure, $P_{op} = 101$ kPa, sheet cavitation occurs at $N = 1200$ rpm, corresponding to $J = 0.166$.

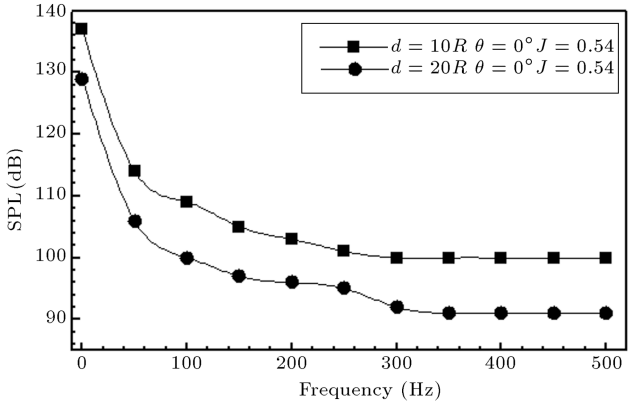

Figure 16. Overall SPLs under non-cavitating conditions for hydrophones 1 and 2 of Model B; $N = 960$ rpm and $V = 2.6$ m/s.

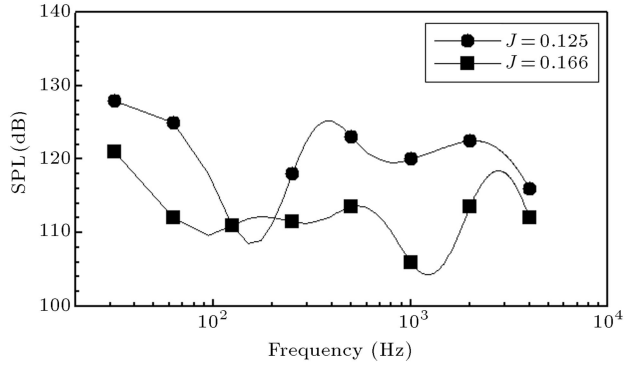

Figure 17. Overall SPLs under sheet cavitation inception and development conditions for Model A at $d = 10R$ and $\theta = 0°$.

Figure 17 shows the overall SPLs under sheet cavitation inception and development conditions for Model A at the distance of 10R from the hub tip. The overall SPLs have been presented at $J = 0.125$ and $J = 0.166$ for the 1/3 octave band at centre frequencies 31.5, 63, 125, 250, 500, 1000, 2000, and 4000 Hz.

The development and increase of sheet cavitation on the blade surface have a great effect on the increase in the overall SPLs. The overall SPLs amplitude difference for the states $J = 0.125$ and $J = 0.166$ changes from 4 to 20 dB in the specific centre frequencies, as seen in Figure 17. Comparing the results for $J = 0.66$ and $J = 0.166$, it can be seen that the overall SPLs amplitude difference between non-cavitating and cavitating cases is 15 to 40 dB in the frequency range of 50-500 Hz, as seen in Figures 14 and 17. The difference between non-cavitating and cavitating conditions in terms of the overall SPLs is comparable with the range of 10 to 30 dB in [25].

5.2.2. Model B

In order to achieve cavitation and observe the vapour volume fraction, decreasing the operating pressure is more significant than increasing the rotational speed.

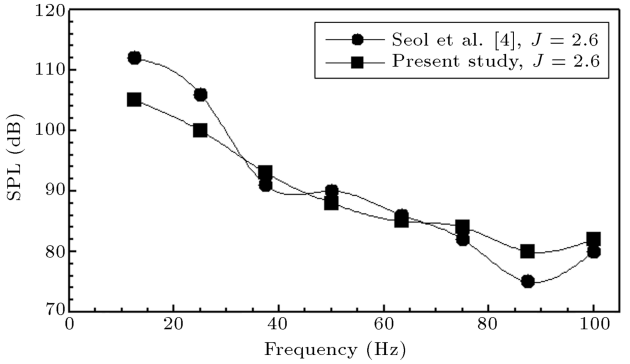

Figure 18. Overall SPLs in $J = 2.6$ for Model B at $d = 10R$ and $\theta = 0°$.

As shown in Figure 11, with an operating pressure of $P_{op} = 101$ kPa, the propeller approaches cavitation at a rotational speed of 1850 rpm. However, if the pressure drops to $P_{op} = 60$ kPa, vapour volume fraction at the propeller tip can be formed at much lower rotational speeds. For example, under operating pressure of $P_{op} = 60$ kPa and the conditions used by Seol [4], very little vapour volume fraction is formed around the tip. Figure 18 compares the results found by Seol to those from our method at a rotational speed of 120 rpm and inlet velocity of 1.6 m/s. As mentioned in the introduction section, RANS codes can predict the velocity distribution of the propeller with a reasonable accuracy. But, the accuracy of the velocity predictions by the panel method is not enough because of the lack of the viscous effect in the theory. Therefore, in a similar condition, our results are more accurate than reference [4].

Figures 19 and 20 represent the overall SPLs under cavitating conditions for the four hydrophones. According to the inverse distance law and comparing the results of the four hydrophones, it was observed that doubling the distance from the sound source decreased the overall SPLs by 6 dB.

Comparing the results in Figures 18 to 20, it can

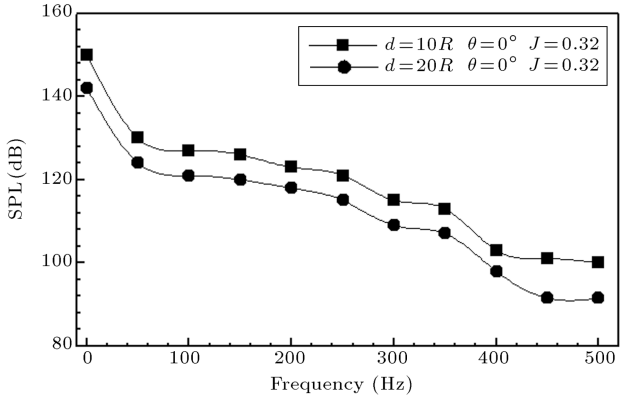

Figure 19. Overall SPLs under cavitating conditions for hydrophones 1 and 2 of Model B; $N = 1850$ rpm and $V = 2.96$ m/s.

Table 2. Comparison between the overall SPLs under different advanced coefficients for Model B.

Frequency	$SPL_{J=0.32}$	$SPL_{J=0.40}$	$SPL_{J=0.60}$	$SPL_{J=0.80}$
100 Hz	128 dB	95 dB	93 dB	89 dB
200 Hz	124 dB	90 dB	88 dB	86 dB
300 Hz	115 dB	86 dB	84 dB	82 dB
400 Hz	104 dB	80.5 dB	78 dB	76 dB
500 Hz	100 dB	76.5 dB	74 dB	72 dB

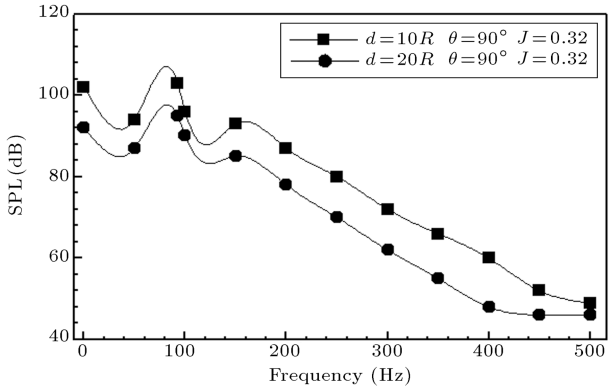

Figure 20. Overall SPLs under cavitating conditions for hydrophones 3 and 4 of Model B; $N = 1850$ rpm and $V = 2.96$ m/s.

be seen that the increase in rotational speed causes a pressure drop on the blade surface, and therefore, sheet cavitation developed on the blade surface. Like that in $J = 0.32$, the amount of cavitation on the blade surface reached its maximum values. In $J = 0.32$ and $P_{op} = 101$ kPa, the overall SPL amplitude increased by about 40 to 50 dB. Table 2 shows a comparison between the obtained overall SPLs under different advanced coefficients at the same frequencies. The overall SPL, under cavitating conditions for $N = 1850$ rpm, and $J = 0.32$ is more than the overall SPL under non-cavitating conditions for $N = 800$ rpm, and $J = 0.4$. This increase in the overall SPLs is due to the sheet cavitation effects and increase in rotational speed.

6. Conclusion

Sheet cavitation is an avoidable physical phenomenon in fluids and has always been a major concern in propeller design. Sheet cavitation is especially common in marine propellers. A reliable and effective numerical technique including sheet cavitation is thus very crucial for the design of marine propellers. This paper presents a numerical study on the non-cavitating and blade sheet cavitation flow analysis of marine propellers. Sheet cavitation is one of the most important propeller noise sources, and therefore, inception and development cavitation conditions should be obtained. Also, in this paper, the overall SPLs are considered and presented under non-cavitating and cavitating conditions.

In this paper, hydrodynamic and noise analyses of two propeller models were studied. Model A is a research propeller used in CEHDMV in Sharif University of Technology. Hydrodynamic tests of this propeller were performed in the k23 cavitation tunnel at CEHDMV. Cavitation occurred for this model at $J = 0.22$ and $P_{op} = 60$ kPa or $J = 0.165$ and $P_{op} = 101$ kPa. Comparing the results for $J = 0.66$ and $J = 0.166$ at $P_{op} = 101$ kPa, it was evident that the overall SPLs amplitude difference under cavitating and non-cavitating conditions was 15 to 40 dB in the frequency range of 50-500 Hz. Also, effects of increase in the rotational speed on sheet cavitation development were considered and results were presented at $J = 0.125$ and $P_{op} = 101$ kPa. The overall SPLs amplitude difference for the states $J = 0.125$ and $J = 0.166$ changed from 4 to 20 dB in the specific centre frequencies.

Model B is a DTMB4119 which has been analysed by several other studies at lower rotational speeds. For this model, a wide range of conditions has been studied and the overall SPLs have been compared under non-cavitating and cavitating conditions in a specific frequency range. Cavitation happened for this model at $J = 0.32$ and $P_{op} = 101$ kPa or at a lower amount of $J = 2.56$ and $P_{op} = 60$ kPa. The amount of sheet cavitation content on the blade surface reaches its maximum values at $J = 0.32$ and $P_{op} = 101$ kPa. For this model, the overall SPLs results were presented at $J = 2.56$, 0.8, 0.6, 0.4, and 0.32. The overall SPLs under cavitating conditions for $N = 1850$ rpm and $J = 0.32$ were more than the overall SPLs under non-cavitating conditions for $N = 800$ rpm and $J = 0.4$. Table 2 shows a comparison between the obtained overall SPLs under different advanced coefficients at the same frequencies. The FW-H equation was solved assuming infinite field and no reflections from the surrounding environment. Therefore, the numerical results of this work can be considered as the net propeller noise measurement results in free-field. Also, by comparison between two propellers, the DTMB 4119 was defined as a propeller that reached cavitation conditions in high rotational speeds. The noise of Model B was higher than the noise of Model A in high rotational speeds and under cavitation conditions, while Model A reached cavitation conditions in lower speeds than Model B. The hydrodynamics of A and B models has

been analysed by others, but a phenomenology study on the noise is carried out widely in the present work for these models.

Nomenclature

$J = V_a/nD$	Advance coefficient
$K_t = T/\rho N^2 D^4$	Thrust coefficient
$K_Q = Q/\rho N^2 D^5$	Torque coefficient
N	Rotating velocity of the propeller
Va	Axis velocity
V_R	Upstream flow velocity
T	Thrust
Q	Torque
α_v	Vapour volume fraction
σ	Cavitation number
P_0	Upstream flow Pressure
P_v	Vapour pressure
P_a	Static pressure
D	Diameter of the propeller
R	Radius of the propeller
h	Static head
θ	Angle relate to hub
$SPLs$	Sound pressure levels
$\sigma_{0.7R}$	Cavitation number in 0.7R
m	Harmonies of the propeller
z	Number of the blade
f_r	Frequency of the shaft
H	Symbol of hydrophone
u_i	Fluid velocity component in the x_i direction
u_n	Fluid velocity component normal to the surface $f = 0$
v_i	Surface velocity components in the x_i direction
v_n	Surface velocity component normal to the surface
$\delta(f)$	Dirac delta function
$H(f)$	Heaviside function

References

1. Ross, D., *Mechanics of Underwater Noise*, Peninsula Publishing, CA: Los Altos (1987).
2. Carlton, J.S., *Marine Propellers and Propulsion*, Butterworth-Heinemann, London (1994).
3. Seol, H., Jung, B., Suh, J.C. and Lee, S. "Prediction of non-cavitation underwater propeller noise", *Journal Sound and Vibration*, **257**(1), pp. 131-157 (2002).
4. Seol, H., Jung, B., Suh, J.C. and Lee, S. "Development of hybrid method for the prediction of underwater propeller noise", *Journal Sound and Vibration*, **288**(1-2), pp. 345-360 (2005).
5. Jin-ming, Y., Ying, X., Fang, L. and Zhan-zhi, W. "Numerical prediction of blade frequency noise of cavitating propeller", *Journal Hydrodynamics*, **24**(3), pp. 371-377 (2012).
6. Pan, Y. and Zhang, H.X. "Numerical prediction of marine propeller noise in non-uniform inflow", *Journal China Ocean Eng.*, **27**, pp. 33-42 (2013).
7. Caro, S., Sandboge, R., Iyer, J. and Nishio, Y. "Presentation of a CAA formulation based on LightHill's analogy for fan noise", *Conference on Fan Noise*, Lyon, France, 17-19 Sep. (2007).
8. Chen, A., Li, S. and Huang, D. "Numerical analysis of aerodynamic noise radiated from cross flow fan", *Journal Energy Power Eng.*, **2**(4), pp. 443-447 (2008).
9. Li, Y., Ouyang, H., Tian, J., Du, Zh. and Zheng, Zhi "Experimental and numerical studies on the discrete noise about the cross-flow fan with block-shifted impellers", *Journal Applied Acoustics*, **71**, pp. 1142-1155 (2010).
10. Lai, H., Wang, M., Yun, C. and Yao, J. "Attenuation of cross-flow fan noise using porous stabilizers", *International Journal of Rotating Machinery*, **2011**(1), pp. 1-10 (2011).
11. Rama, K.S., Rama, K.A. and Ramji, K. "Reduction of motor fan noise using CFD and CAA simulations", *Journal Applied Acoustics*, **72**, pp. 982-992 (2011).
12. Gue, F., Cheong, Ch. and Kim, T. "Development of low-noise axial cooling fans in a household refrigerator", *Journal of Mechanical and Technology*, **25**(12), pp. 2995-3004 (2011).
13. Li, W. and Yang, C. "Numerical simulation of flow around a podded propeller", *Proceedings of the Nineteenth International Offshore and Polar Engineering Conference*, pp. 756-762, Osaka, Japan, June 21-26 (2009).
14. Subhas, S., Saji, V.F., Ramakrishna, S. and Das, H.N. "CFD analysis of a propeller flow and cavitation", *International Journal of Computer Applications*, **55**(16), pp. 26-33 (2012).
15. Sanchez-Caja, A. "P4119 RANS calculations at VTT", 22nd ITTC Propeller RANS/Panel Method Workshop, France (1998).
16. Bagheri, M.R., Seif, M.S. and Mehdigholi, H. "Numerical simulation of underwater propeller noise", *Journal of Ocean, Mechanical and Aerospace - Science and Engineering*, **4**, pp. 1-6 (2014).
17. Bagheri, M.R., Seif, M.S. and Mehdigholi, H. "Noise and Hydrodynamic analysis of submerged propeller by numerical method", *5th Offshore Industries Conference*, Iran, Sharif University of Technology (2013).
18. Senocak, I. and Shyy, W. "Numerical simulation of

turbulent flows with sheet cavitation", *Department of Aerospace Engineering, Mechanics and Engineering Science*, University of Florida, Florida (2001).

19. Pereira, F., Salvatore, F. and Di Felice, F. "Measurement and modelling of propeller cavitation in uniform inflow", *Journal of Fluids Engineering*, **126**, pp. 671-679 (2004).
20. Bernad, S. "Numerical analysis of the cavitating flows", *Center of Advanced Research in Engineering Sciences*, Romania Academy, Timisoara Branch, Romania (2006).
21. Sridhar, D., Bhanuprakash, T.V.K. and Das, H.N. "Frictional resistance calculations on a ship using CFD", *Int. J. of Computer Applications*, **11**(5), pp. 24-31 (2010).
22. Salvatore, F., Greco, L. and Calcagni, D. "Computational analysis of marine propeller performance and cavitation by using an inviscid-flow BEM model", *Second International Symposium on Marine Propulsors smp'11*, Hamburg, Germany (2011).
23. Zhi-feng, ZHU and Shi-liang, FANG "Numerical investigation of cavitation performance of ship propellers", *Journal of Hydrodynamics*, Ser. B, **24**(3), pp. 347-353 (2012).
24. "Cavitation and powering performance", The Propulsion Committee, *Final Report and Recommendations to the 22nd ITTC* (1998).
25. Sharma, S.D., Mani, K. and Arakeri, V.H. "Cavitation noise studies on marine propellers", *Journal Sound and Vibration*, **138**(2), pp. 255-283 (1990).
26. Atlar, M., Takinaci, A.C., Korkut, E., Sasaki, N. and Aono, T. "Cavitation tunnel tests for propeller noise of a FRV and comparisons with full-scale measurements", In: *CAV Fourth International Symposium on Cavitation* (2001).
27. Park, C., Seol, H., Kim, K. and Seong, W. "Study propeller noise source localization in a cavitation tunnel", *Journal Ocean Engineering*, **36**, pp. 754-762 (2009).
28. Bagheri, M.R., Seif, M.S. and Mehdigholi, H. "An analysis of hydrodynamics and noise behavior for submerged propeller in various conditions by experimental and numerical methods", *Journal Modares Mechanical Engineering*, **14**(5), pp. 15-25 (2014).
29. Lighthill, M.J. "On sound generated aerodynamically. II. Turbulence as a source of sound", *Proc. Roy. Soc. Lond*, A 222, pp. 1-22 (1954).
30. Ffowcs Williams, J.E. and Hawkings, D.L. "Sound generated by turbulence and surfaces in arbitrary motion", *Philosophical Transactions of the Royal Society A*, **264**(1151), pp. 321-342 (1969).
31. Farassat, F. and Brentner, K.S. "Modeling aerodynamically generated sound of helicopter rotors", *Proc. Roy. Soc.*, USA VA, **23681**, pp. 94-96 (2003).
32. Zwart, P.J., Gerber, A.G. and Belamri T. "A two phase flow model for predicting cavitation dynamics", In *ICMF 2004 International Conference on Multiphase Flow*, Yokohama, Japan, May 30 - June 3 (2004).
33. Ivanell, S. "Hydrodynamic simulation of a torpedo with pump jet propulsion system", Master Thesis, Stockholm (2001).
34. Kulczyk, J., Skraburski, L. and Zawislak, M. "Analysis of screw propeller 4119 using the fluent system", *Archives of Civil and Mechanical Engineering*, **7**(4), pp. 129-136 (2001).
35. Arazgaldi, R., Hajilouy, A. and Farhanieh, B. "Experimental and numerical investigation of marine propeller cavitation", Sharif University of Technology, *Journal Scientia Iranica*, **16**(6), pp. 525-533 (2009).
36. Jessup, S.D. "An experimental investigation of viscous aspects of propeller blade flow", Ph.D. Thesis, School of Engineering and Architecture, the Catholic University of America (1989).
37. Jacobsen, F., Poulsen, T. and Rindel, J.H. "Fundamentals of acoustics and noise control", Note no 31200, Department of Electrical Engineering, Technical University of Denmark September (2011).

Biographies

Mohammad Reza Bagheri received the BSc degree in Mechanical Engineering from Mashhad University, Mashhad, Iran, in 2007, and the MSc degree in Marine Engineering from Malek-Ashtar University of Technology, Tehran, Iran, in 2010. He is currently a PhD student at the School of Mechanical Engineering in Sharif University of Technology, Tehran, Iran. His research interest is the hydrodynamics and acoustics of marine propellers. He has published several papers in this field.

Mohammad Saeed Seif received the BSc degree in Mechanical Engineering from Amirkabir University of Technology, Tehran, Iran, in 1989; the MSc degree in Naval Architecture from Technical University of Gdansk, Gdansk, Poland, in 1992, and the PhD degree in Mechanical Engineering from Yokohama National University, Yokohama, Japan, in 1995. He is currently Professor at the Department of Mechanical Engineering in Sharif University of Technology, Tehran, Iran. His areas of expertise are Dynamics and Hydrodynamics of Marine Vehicles, Ship structure design, advanced marine vehicles, and advanced fluid dynamics. He has published several papers in the acoustic field.

Hamid Mehdigholi received the BS degree in Mechanical Engineering from Sharif University, Tehran, in 1977, and the MS and PhD degrees in Applied Mechanics from the Imperial College, London, in 1986 and 1991, respectively. He has been a faculty member

in Sharif University of Technology since 1991. His research interests include dynamics of rotating machines, vibration isolation, acoustics, and experimental modal analysis. He has published several papers in the acoustic field.

Omar Yaakob received the BSc degree in the field of Marine Engineering from Newcastle-Upon-Tyne in 1983, the MSc degree in the field of Marine Technology from Newcastle-Upon-Tyne in 1987, and PhD in the field of Seakeeping Design from Newcastle-Upon-Tyne, in 1999. He is currently Professor at the Department of Marine Engineering in University Technology Malays. His areas of expertise are Marine technology, Ship design, Shipbuilding, Hydrodynamics, and Marine Structures.